Full Paper Wiley Online Library ELECTROANALYSIS

DOI: 10.1002/elan.201400397

Range of Validity of a Simplified Model for Diffuse Charge Dynamics

Mengying Li,[a] Howard H. Hu,*[a] and Haim H. Bau[a]

Abstract: The modelling of electrochemical processes often requires the solution of the Poisson-Nernst-Planck (PNP) equations. In complex geometries, such as porous electrodes, that is challenging due to the presence of disparate length scales, ranging from the Debye screening length (~nm) to the device length scale (~cm). To overcome this difficulty, one often assumes that the electric double layer (EDL) is at quasi-equilibrium to construct a simplified model that accounts for ion diffusion in the electro-neutral bulk of the electrolyte while replacing the EDLs with appropriate boundary conditions. Various researchers have demonstrated that such an approach is valid in the asymptotic limit of a thin EDL and moderate electrode potentials. In this note, we explore the range of validity of this approximation by considering a one-dimensional electrolytic cell with blocking electrodes subjected to a step change and time-periodic alternations in the electrodes' potentials by calculating the errors associated with the approximate approach as functions of the EDL thickness and electric field frequency and intensity. Additionally, we delineate numerical instabilities associated with the numerical solutions of the bulk equations with the nonlinear boundary condition peculiar to this problem.

Keywords: Electric double layer · Debye screening length · Diffuse charge dynamics · Electric field · Step change · AC

1 Introduction

Mathematical modelling of electrochemical systems is of interest in diverse technologies, ranging from energy storage devices such as batteries and supercapacitors to desalination reactors to colloidal systems [1–5]. Mathematical models that account for mass transfer in the electrolyte consist of the Poisson-Nernst-Planck (PNP) equations, with occasional modifications to account for the finite size of the ions (steric effects) and the presence of a compact (Stern) layer next to solid surfaces [6,7]. The numerical solution of the PNP equations in multi-dimensional settings and complex geometries, such as porous electrodes [1,3,4,8], is complicated due to the presence of disparate length scales. The region next to the solid surface consists of a diffuse (Gouy-Chapman) charged layer, just a few nanometers thick, while the system's overall dimensions may be on the millimetre scale or even larger. The need to accurately resolve the electric double layers next to solid surfaces imposes considerable demands on computational resources. To overcome this difficulty, various researchers [9] decomposed the electrolyte solution into two regions - an inner domain comprised of the electric double layer (EDL) and an outer, electroneutral, bulk region - and used matched, singular asymptotic expansions to determine the potential and concentration fields in the electrolyte. Bazant et al. [10] provided a detailed exposition of the dynamics of the diffuse layer in a one-dimensional system confined between a pair of blocking (perfectly-polarizable) electrodes subjected to a step change in the electrodes' potential difference and a lucid review and historical perspective of the pertinent literature. Olesen et al. [11] studied in detail a one-dimensional electrolytic cell subjected to periodic alternations in the electrodes' potentials. In the above two cases [10,11], a range of parameters exists when the EDL can be considered to be nearly at equilibrium and the bulk solution can be treated as electrically neutral. Under these circumstances, one can use the equilibrium distributions of the ions in the electric double layers to obtain expressions for the charge and the number of ions in the EDL as functions of the electrodes' potentials and then use these expressions as boundary conditions for the bulk equations. Although this simplified model is often used [10,11], a systematic study of its range of applicability and numerical analysis of the solution of the bulk equations appears to be lacking.

In this note, we examine the range of validity of a simplified model that accounts for the electrochemical processes in the bulk of the electrolyte, while replacing the EDL with appropriate boundary conditions. We consider a one-dimensional electrolytic cell confined between two blocking electrodes subjected to a step change in the potential difference and to temporally alternating potential. In departure from the analytical treatments, we allow for the concentration of the electrolyte in the outer (bulk) region to vary in space and time, so that the EDL charging is coupled to bulk diffusion. By comparing the predictions of our simplified model with those of the complete PNP equations, we determine the error incurred by the approximate solution as a function of the Debye screen-

[a] M. Li, H. H. Hu, H. H. Bau
Department of Mechanical Engineering and Applied Mechanics, University of Pennsylvania
*e-mail: hhu@seas.upenn.edu

ing length, the electrode potential, and the period of the temporal alternation in electrode potential. Our objectives are to inform modellers under what conditions the quasi-equilibrium treatment of the EDL is reasonable and to identify the magnitude of the errors associated with the approximations. In the course of our study, we have identified numerical instabilities associated with the solution of the bulk, diffusion equations subject to nonlinear boundary conditions. We examine the origins of these instabilities in an appendix.

2 Mathematical Model

2.1 Poisson-Nernst-Planck Model

Consider a dilute z_1:z_2, binary electrolyte solution confined in the one-dimensional cell $-L \le X \le L$ bordered by two perfectly polarizable (blocking) electrodes (Figure 1). In the absence of an electric field, the uniform cations (valence z_1) and anions (valence z_2) concentrations are, respectively, $C_{1,0}$ and $C_{2,0}$. The left and right electrodes are, respectively, subjected to potentials $\phi_w(\tau)/2$ and $\phi_w(\tau)/2$.

Conservation of species requires that the concentrations of the ions satisfy the Nernst-Planck equation

$$\frac{\partial C_i}{\partial \tau} = \frac{z_i D_i F}{RT}\frac{\partial}{\partial X}\left(C_i \frac{\partial \phi_e}{\partial X}\right) + D_i \frac{\partial^2 C_i}{\partial X^2}, \tag{1}$$

where $i=1$ and $i=2$ denote, respectively, the cations and anions. $C_i(X,t)$ (mol/m^3) is the concentration of species i, τ is time, D_i is the diffusion coefficient of species i, F is the Faraday constant, R is the universal gas constant, T is the absolute temperature, and $\phi_e(\tau)$ is the electrical potential in the electrolyte solution.

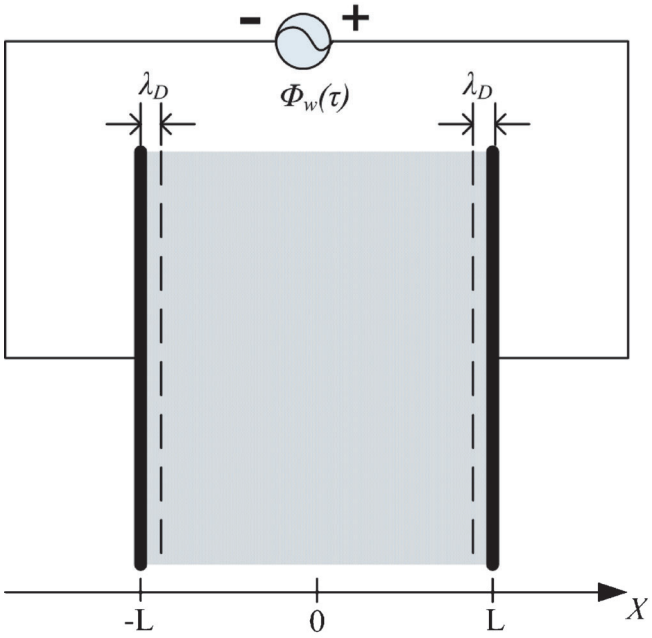

Fig. 1. A schematic depiction of the liquid cell $-L \le X \le L$.

The potential field satisfies the Poisson equation

$$\frac{\partial^2 \phi_e}{\partial X^2} = -\frac{\widehat{\rho}_E}{\epsilon}, \tag{2}$$

where $\widehat{\rho}_E = F(z_1 C_1 + z_2 C_2)$is the volumetric charge density, and ϵ is the dielectric permittivity of the solvent. It is convenient to define the average concentration $C=(1/2)[(C_1/\nu_1)+(C_2/\nu_2)]$ where ν_1 and ν_2 are, respectively, the number of cations and anions produced when a solute molecule dissociates. The ν_1 and ν_2 are related to the ions' valances through $z_1\,\nu_1 + z_2\,\nu_2 = 0$.

Next, we recast the equations in dimensionless form. Unless otherwise stated, we adopt the convention that lower case letters are the dimensionless counterpart of the dimensional quantities written with capital letters. L is the length scale; $C_0=(1/2)\,[(C_{1,0}/\nu_1)+(C_{2,0}/\nu_2)]$ is the concentration scale; the thermal potential RT/z_1F is the potential scale; and $2Fz_1C_0$ is the charge density scale. We use the RC time constant $\tau_{RC}=\lambda_D L/D_1$ as the time scale [10]. In the above, $\lambda_D=(\epsilon RT/2F^2 z_1{}^2 C_0)^{1/2}$ is the Debye screening length. We also define $\alpha=D_2/D_1$, $\beta=z_2/z_1$, and $\nu_2=-\nu_1/\beta$. Accordingly, $c_1=\rho_e+c\nu_1$ and $c_2=(\rho_e-c\nu_1)/\beta$. For brevity, in this study we consider only a symmetric ($\beta=-1$), mono-valent ($\nu_1=1$), binary electrolyte with the anions and cations having the same diffusivities ($\alpha=1$).

The resulting dimensionless equations, expressed in terms of c and ρ_e

$$\frac{\partial c}{\partial t} = \epsilon\frac{\partial}{\partial x}\left(\rho_e\frac{\partial \phi_e}{\partial x} + \frac{\partial c}{\partial x}\right), \tag{3}$$

$$\frac{\partial \rho_e}{\partial t} = \epsilon\frac{\partial}{\partial x}\left(c\frac{\partial \phi_e}{\partial x} + \frac{\partial \rho_e}{\partial x}\right), \tag{4}$$

and

$$\frac{\partial^2 \phi_e}{\partial x^2} = -\frac{\rho_e}{\epsilon^2}, \tag{5}$$

apply when $-1 \le x \le 1$ and for $t>0$, where $\epsilon=\lambda_D/L$. The impermeable boundary conditions at the electrodes' surfaces ($x=\pm 1$) imply:

$$\rho_e\frac{\partial \phi_e}{\partial x} + \frac{\partial c}{\partial x} = 0, \tag{6}$$

and

$$c\frac{\partial \phi_e}{\partial x} + \frac{\partial \rho_e}{\partial x} = 0. \tag{7}$$

The boundary conditions for the potential are

$$\phi_e(\pm 1,t)=\pm\left(\frac{1}{2}\phi_w(t)-\delta\cdot\epsilon\frac{\partial\phi_e(\pm 1,t)}{\partial x}\right). \quad (8)$$

The initial conditions are:

$$c(x,0)=\rho_e(x,0)=0 \text{ and a given } \phi_e(x,0). \quad (9)$$

In the above, $\delta=\lambda_S/\lambda_D$ and λ_S is the Stern layer's thickness.

When a temporally varying potential is applied across the electrodes, electrical current flows through the external circuit that connects the electrodes to a power supply/load and the electrodes charge/discharge. The dimensionless electrical current in the external circuit per unit area of the electrode is

$$j^{exact}(t)=\frac{\partial}{\partial t}\left(\epsilon\frac{\partial\phi_e}{\partial x}\right)_{x=-1}. \quad (10)$$

In the above, the current scale is $2FzC_0D/L$.

The mathematical model comprised of Equations 3–5 involves two length scales: the $O(1)$ length of the electrolyte cell and the $O(\epsilon)$ length of the Debye screening length. When one is solving the PNP equations in multi-dimensional settings and/or complex geometries such as porous electrodes, it may not be practical to resolve length scales down to $O(\epsilon)$. When the temporal variations in the electrodes' potentials are relatively slow such that the charge relaxation time of the EDL, $\tau_d=\lambda_D^2/D$, is much smaller than the RC time of the electrolytic cell $\tau_{RC}=\lambda_D L/D$, it may be reasonable to assume that the EDL is at quasi-equilibrium.

2.2 Quasi-Equilibrium Electric Double Layer

In this section, we consider a quasi-equilibrium EDL and neglect the Stern layer ($\lambda_S=0$) and the ions' volume. By neglecting the Stern layer and steric effects, we are putting the quasi-equilibrium approximation to a more severe test than when these effects are included. The analysis can, however, be extended to account for these neglected effects.

We use a singular perturbation expansion. We divide the domain $-1\le x\le 1$ into two EDLs, each of thickness ϵ and a core (bulk) region. Superscripts EDL and B denote, respectively, the EDL variables and the bulk variables. In the EDL, we introduce the stretched coordinate $\xi=(1+x)/\epsilon$ next to the left boundary ($x=-1$). The dimensionless PNP equations in the left EDL assume the form:

$$\epsilon\frac{\partial c^{EDL}}{\partial t}=\frac{\partial}{\partial\xi}\left(\rho_e^{EDL}\frac{\partial\phi_e^{EDL}}{\partial\xi}+\frac{\partial c^{EDL}}{\partial\xi}\right), \quad (11)$$

$$\epsilon\frac{\partial\rho_e^{EDL}}{\partial t}=\frac{\partial}{\partial\xi}\left(c^{EDL}\frac{\partial\phi_e^{EDL}}{\partial\xi}+\frac{\partial\rho_e^{EDL}}{\partial\xi}\right), \quad (12)$$

and

$$\frac{\partial^2\phi_e^{EDL}}{\partial\xi^2}=-\rho_e^{EDL}. \quad (13)$$

The boundary conditions at $\xi=0$ or ($x=-1$) are:

$$\rho_e^{EDL}\frac{\partial\phi_e^{EDL}}{\partial\xi}+\frac{\partial c^{EDL}}{\partial\xi}=0, \quad (14)$$

$$c^{EDL}\frac{\partial\phi_e^{EDL}}{\partial\xi}+\frac{\partial\rho_e^{EDL}}{\partial\xi}=0, \quad (15)$$

and

$$\phi_e^{EDL}=-\frac{1}{2}\phi_w. \quad (16)$$

To the first order of approximation, the matching conditions at the right edge of the LHS EDL are:

$$\lim_{\xi\to\infty}\begin{pmatrix}c^{EDL}(\xi,t)\\ \phi_e^{EDL}(\xi,t)\end{pmatrix}=\lim_{x\to -1}\begin{pmatrix}c^{B}(x,t)\\ \phi_e^{B}(x,t)\end{pmatrix}.$$

To the leading order $\epsilon\to 0$, we drop the time-derivatives from Equations 11–13. The cation and anion concentration fields satisfy, respectively, the Boltzmann distributions

$$c_1^{EDL}(\xi,t)=c_1^B(-1,t)\exp\left(-\phi_e^{EDL}(\xi,t)+\phi_e^B(-1,t)\right)$$

and

$$c_2^{EDL}(\xi,t)=c_2^B(-1,t)\exp\left(\phi_e^{EDL}(\xi,t)-\phi_e^B(-1,t)\right)$$

Accordingly [12,13],

$$c^{EDL}(\xi,t)=c^B(-1,t)\cosh\left(\phi_e^{EDL}(\xi,t)-\phi_e^B(-1,t)\right), \quad (17)$$

and

$$\rho_e^{EDL}(\xi,t)=\frac{1}{2}c_1^B(-1,t)\sinh\left(\phi_e^{EDL}(\xi,t)-\phi_e^B(-1,t)\right). \quad (18)$$

The potential field in the EDL is obtained by integrating the Poisson-Boltzmann Equation 13 twice [11].

$$\phi_e^{EDL}(\xi,t)=\phi_e^B(-1,t)+$$

$$4\tanh^{-1}\left[e^{-\sqrt{c^B(-1,t)}\xi}\tanh\left(\frac{\zeta^-}{4}\right)\right], \quad (19)$$

where the zeta potential $\zeta^-(t)=-\frac{1}{2}\phi_w(t)-\phi_e^B(-1,t)$.

The structure of the right hand side EDL ($x=1$) can be obtained in a similar manner. In the above and later, su-

perscripts (−) and (+) denote, respectively, the left and right EDLs.

2.3 Bulk Electrolyte

In the bulk region outside the EDLs, Equation 5 predicts $\rho_e^{B} \sim O(\epsilon^2)$. Therefore, we enforce charge neutrality, $\rho_e^{B} = 0$. Accordingly, Equations 3–4 reduce to

$$\frac{\partial c^B}{\partial t} = \epsilon \frac{\partial^2 c^B}{\partial x^2} \tag{20}$$

and

$$\frac{\partial}{\partial x}\left(c^B \frac{\partial \phi_e^B}{\partial x}\right) = 0 \tag{21}$$

with the initial conditions $c^{B}(x,0)=1$ and $\phi_e^{B}(x,0)=\phi_w(0)x/2$. The presence of ϵ in Equation 20 indicates that the bulk concentration field relaxes slowly with diffusive time scale $\tau_L = \tau_{RC}/\epsilon = L^2/D$. In contrast, time does not enter explicitly into the potential Equation 21. The bulk potential field adjusts instantaneously to variations in the boundary data.

Next, we introduce the boundary conditions of the bulk Equations 20 and 21. Since the EDLs act as sinks/sources for ions and charges, the bulk experiences mass and charge fluxes through its boundaries ($x=\pm 1$). The total charge $q^{\pm}(t)$ in the EDLs is obtained by integrating Equations 13 and 19 across the EDL.

$$q^{\pm}(t) = \int_0^{\infty} \rho_e^{EDL} \mathrm{d}\xi = -2\sqrt{c^B(\pm 1,t)}\sinh\left(\frac{\xi^{\pm}}{2}\right), \tag{22}$$

where we used $\sqrt{2\epsilon RTC_0}$ as the charge scale.

The concentration of the excess ions in the EDL is:

$$c^{\pm EDL}(\xi,t) = \frac{1}{2}\left(c_1^{EDL}(\xi,t) - c_1^B(\pm 1,t) + c_2^{EDL}(\xi,t) - c_2^B(\pm 1,t)\right).$$

Upon integration over the EDL's thickness, the total number of excess ions

$$w^{\pm}(t) = \int_0^{\infty} c^{\pm EDL} \mathrm{d}\xi = 4\sqrt{c^B(\pm 1,t)}\sinh^2\left(\frac{\xi^{\pm}}{4}\right). \tag{23}$$

The boundary conditions for the bulk equations are:

$$\left[\frac{\partial}{\partial x} c^B\right]_{x=\pm 1} = \mp \frac{\mathrm{d}}{\mathrm{d}t} w^{\pm}(t) \tag{24}$$

and

$$\left[c^B \frac{\partial}{\partial x}\phi_e^B\right]_{x=\pm 1} = \mp \frac{\mathrm{d}}{\mathrm{d}t} q^{\pm}(t). \tag{25}$$

2.4 Composite Expressions

It is convenient to construct composite expressions that are uniformly valid in the entire domain. To this end, we add the expressions in the EDL and the bulk and subtract the overlapping contributions to obtain the uniformly valid approximations

$$\phi_e^{comp}(x,t) = \phi_e^B(x,t) + 4\tanh^{-1}\left[e^{-\sqrt{c^B(\mathrm{sgn}(x),t)}\frac{1-\mathrm{sgn}(x)x}{\epsilon}}\tanh\left(\frac{\xi^{\mathrm{sgn}(x)}}{4}\right)\right], \tag{26}$$

$$c^{comp}(x,t) = c^B(x,t)\cosh\left(\phi_e^{comp}(x,t) - \phi_e^B(x,t)\right),$$

and

$$j^{comp} = \frac{\partial}{\partial t}\left(\epsilon \frac{\partial \phi_e^B}{\partial x}(-1,t) - 2\sqrt{c^B(-1,t)}\sinh\left(\frac{\xi^-}{2}\right)\right).$$

Similar expressions have been previously presented in Bazant et al. [10] as the leading order terms in asymptotic expansions. The main difference between our expressions and Bazant et al. [10] is that we allow for time-dependent bulk concentration. We anticipate that the approximate (outer) model will fail when the EDL is thick and/or when the electrodes' potential difference is large. When the potential difference is large, one needs to account for the finite size of the ions (steric hindrance) and the classical PNP model is no longer valid [6,7]. We will systematically explore the error incurred in using the approximate model as a function of the EDL thickness and the magnitude of the electrodes' potential difference.

3 Results and Discussion

We will determine, through numerical simulations, the range of applicability of the approximate model (Section 2.3–2.4) by comparing its predictions with those of the PNP equations (Section 2.1). We consider the electrochemical cell depicted schematically in Figure 1 when the electrodes are subjected to both a step change (section 3.1) and time-periodic variations in potential (Section 3.2).

Both the exact and approximate models were solved with the COMSOL Multiphysics Finite Element Program. The exact model (Equations 3–5) was implemented using the "General Form PDE" module with zero flux and Dirichlet boundary condition. Nonuniform elements with sufficiently fine mesh next to the electrode surfaces were introduced to resolve the electric double layer. The approximate model (Equations 20 and 21) was first converted to the weak formulation, and implemented using the "Weak Form PDE" module. The boundary conditions

(Equations 24 and 25) were added as "Weak Contribution" at the corresponding boundary nodes. A uniform mesh was used in the solution. In both cases, we verified that the computational results were grid size-independent and that the numerical solutions matched analytical ones in limiting cases and results reported in the literature, when available.

3.1 Step Change in Electrode Potential

At time $t=0$, the electrodes are subjected to a step change in potential:

$$\phi_w(t) = \phi_p H(t)$$

where $H(t)$ is the Heaviside step function ($H(t)=0$ when $t<0$ and $H(t)=1$ when $t\geq 0$) and ϕ_p is the magnitude of the potential step. The initial conditions are $c^B(x,0)=1$ and $\phi_\epsilon^B(x,0)=\phi_p\, x/2$.

The dynamics of a binary, symmetric electrolyte subjected to a step change in the electrodes' potentials, accounting for a finite Stern layer effect ($\delta>0$), was studied by Bazant et al[10]. In our model, the EDL charging is coupled to the bulk diffusion and characterized as the strongly nonlinear dynamic regime [10].

The approximate (outer) bulk model (Equations 20 and 21) admits the steady-state (long time) solution

$$c^B(x,\infty) - c^B_\infty = \phi^B_e(x,\infty) = 0. \tag{29}$$

Integrating Equation 20 over time and across the electrochemical cell and considering mass conservation, we find

$$\sqrt{c^B_\infty} = \sqrt{1+4\epsilon^2\sinh^4\left(\phi_p/8\right)} - 2\epsilon\sinh^2\left(\phi_p/8\right). \tag{30}$$

When $\phi_p \ll 1$ and $\phi_p \gg 1$, Expression 30 reduces, respectively, to

$$c^B_\infty \approx 1 - \frac{\epsilon}{16}\phi_p^2 + O\left(\phi_p^4\right) \text{ and } c^B_\infty \approx 1/\epsilon^2 e^{-\phi_p/2}. \tag{31}$$

The corresponding total charge accumulated in the EDL

$$q_\infty = q(\infty) = 2\sqrt{c^B_\infty}\sinh\left(\phi_p/4\right) \tag{32}$$

is obtained from Equation 22. In the limit of a small and large ϕ_p, Expression 32 reduces, respectively, to

$$q_\infty = \phi_p/2 + O\left(\phi_p^3\right) \text{ and } q_\infty = q_{\max} \approx 1/\epsilon. \tag{33}$$

The latter value corresponds to the dimensional charge

$$Q_{\max} = \sqrt{2\epsilon RTC_0}\frac{L}{\lambda_D} = 2FzC_0L,$$

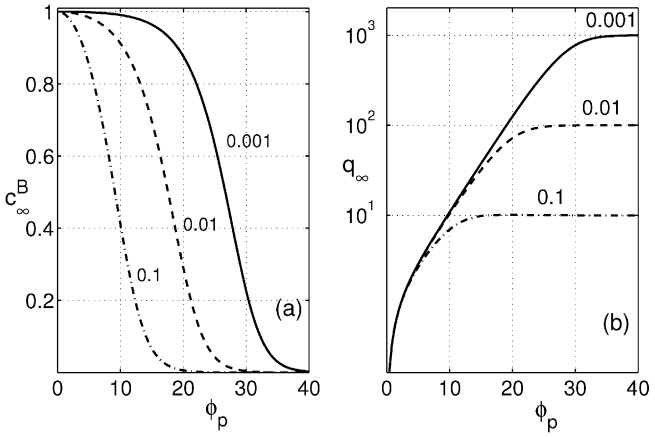

Fig. 2. Steady state concentration c^B_∞ (a) and the total charge accumulated in EDL q_∞ (b) as functions of applied potential difference ϕ_p. $\epsilon=0.1$, 0.01, and 0.001.

which is the total charge available in the cell. In other words, when ϕ_p is sufficiently large, all the charge will be packed into the corresponding EDLs.

Figure 2 depicts the steady state concentration c^B_∞ and the total charge in the EDL q_∞ as functions of applied potential ϕ_p when $\epsilon=0.1$, 0.01, and 0.001. The plateaus in q_∞ (Figure 2b) correspond to circumstances when all the ions accumulated in the EDL ($c^B_\infty \approx 0$). The asymptotic results for large ϕ_p may not be of practical significance since our model does not account for overcrowding in the EDL.

When the amplitude of the wall potential is small, $\phi_p \ll 1$, we linearize the boundary conditions and solve the bulk equations analytically.

$$\phi^B_e(x,t) = \frac{1}{2}\phi_p x e^{-t} + O\left(\phi_p^3\right) \tag{34}$$

and

$$c^B(x,t) = 1 + \phi_p^2 c_2(x,t) + O\left(\phi_p^4\right) \tag{35}$$

where

$$c_2(x,t) = \frac{\sqrt{\epsilon}}{8}\left(\frac{\cos(x/\sqrt{\epsilon})}{\sin(1/\sqrt{\epsilon})}e^{-t} - \frac{\cos\left(x\sqrt{2/\epsilon}\right)}{\sqrt{2}\sin\left(\sqrt{2/\epsilon}\right)}e^{-2t}\right)$$
$$-\frac{\epsilon}{16} - \frac{\epsilon}{4}\sum_{n=1}^{\infty}\frac{(-1)^n\cos(n\pi x)e^{-n^2\pi^2\epsilon t}}{(n^2\pi^2\epsilon-1)(n^2\pi^2\epsilon-2)}$$

We used the above expressions to verify our numerical solutions.

To assess the approximate model's validity, we define the relative error (E) between the exact (Equation 10) and approximate (Equation 28) currents at the electrodes:

$$E_m = \max_t |E(t)| = \max_t \left| \frac{j^{exact}(t) - j^{comp}(t)}{j^{exact}_{max}} \right| \quad (36)$$

When $\phi_p \leq 1$ and $\epsilon = 0.05$, the approximate model, exact model, and the perturbation solution (Equations 34 and 35) are in good agreement. $E_m < 1.5\,\%$.

Figure 3 compares the predictions of the exact and approximate models when $\phi_p = 8$ and $\epsilon = 0.05$. These particular values were selected to allow comparison with the results reported in Bazant et al[10]. Moreover, the relatively thick EDL allows us to depict the differences between the approximate composite solution and the exact solution. Figs. 3a and 3b depict, respectively, the potential and concentration distributions at various times. Since the potential field is antisymmetric $(\phi_e(-x,t) = -\phi_e(x,t))$ and the concentration field is symmetric $(c(-x,t) = c(x,t))$ with respect to $x = 0$, only half the region $-1 \leq x \leq 0$ is shown in Figure 3. When a potential difference is initially applied across the electrodes ($t \sim 0$), the potential distribution in the bulk solution is linear. As the EDL builds up, the electric field is screened by the double layers and the bulk potential gradually reduces to zero. Figure 3b illustrates the penetration of the diffusion front into the bulk of the solution as ions accumulate in the EDL. The bulk concentration varies non-monotonically from its initial uniform value $c(x,0) = 1$ to the asymptotic, long-time value c^B_∞. At intermediate times, the concentration $c^B(-1,t)$ dips below its long time, asymptotic value.

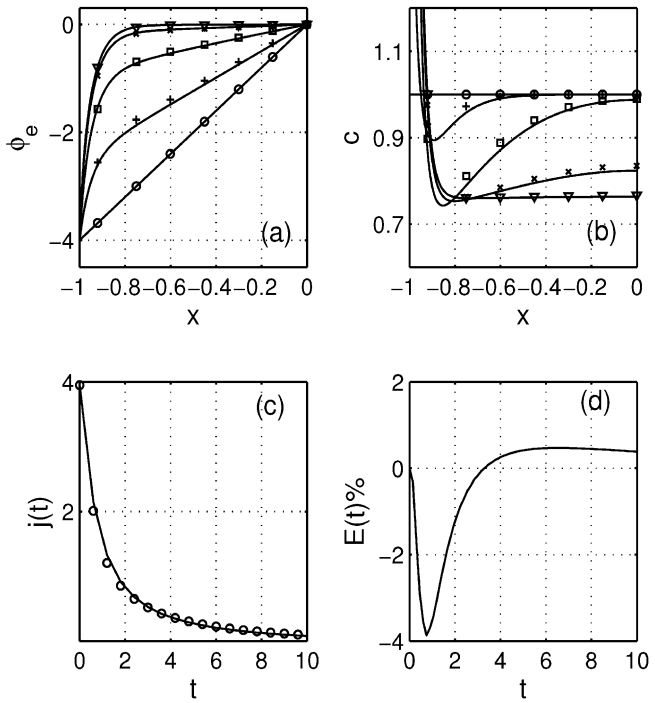

Fig. 3. Comparison of the approximate (symbols) and exact (solid lines) solutions. $\phi_p = 8$ and $\epsilon = 0.05$. The potential (a) and the concentration (b) are depicted as functions of x at times $t = 0$ (○), 0.5 (+), 2 (□), 8 (×), and 20 (▽). The external current flux (c) and the discrepancy between the exact and approximate external currents (d) are depicted as functions of time.

Figure 3c depicts the external current predicted by the exact model (Equation 10, solid line) and the approximate model (Equation 28, hollow circles) as functions of time. In practice, when an external power supply is connected to the electrodes, the initial charging dynamics will be controlled by the external resistance and the electrode potential will increase gradually from zero to its final value. Here, we consider the limiting case of no external resistance. As a result, the exact model predicts infinite current at $t = 0$. In contrast, the finite element simulation smoothes the step change in potential, which results in a finite current at $t = 0$. As time increases, the current decays. At $t = 0$, the electrolytic cell has a capacitance of $C_{cp}(0) = \epsilon$ per unit area of the electrode. As the EDL builds up, the cell's dimensional capacitance increases to the steady state value of $C_{cp}(\infty) = 8\ F^2\ z^2\ C_0\ \sqrt{c^B_\infty}\ \sinh(\phi_p/4)/(RT\phi_p)$.

Figure 3d depicts the discrepancy $E(t)$ (Equation 36) between the approximate and exact predictions for the external current as a function of time. The approximate and exact solutions agree within $E_m < 4\,\%$ at all times and are also in agreement with Figures 10a and 10c of Bazant et al. [10]. The minor differences between our solutions and Bazant et al's are due to our calculations excluding the Stern layer.

We repeated the calculations for various values of ϕ_p and ϵ. Since we excluded the Stern layer, the bulk electrolyte was exposed to much higher potentials that it would have been in the presence of a Stern layer. In other words, by excluding the Stern layer, we put the model to a more severe test than in the presence of the Stern layer. Figure 4 depicts the contours of the relative error (E_m) as a function of ϕ_p and ϵ. The regions beneath the solid curves identify the parameter space when the error is smaller than the indicated magnitude, such that the approximate model is applicable. As ϕ_p and ϵ decrease, so does the error of the approximate model. For the parameters in the space above the curves, one has to rely on the solution of the full PNP equations.

At moderate values of ϕ_p and ϵ, the numerical solution of the nonlinear bulk model encounters convergence difficulties, presenting a challenge to numerical analysts. We describe briefly the numerical stability issues below and in more details in the appendix.

Since our model does not account for the ions' finite size, high electrode potentials lead to a very rapid depletion of ions from the bulk region's edge and exceedingly low local salt concentration $c^B(-1,t)$. Figure 3b provides a mild example of this behaviour. To avoid the concentration $c^B(-1,t)$ from attaining non-physical, negative values, one must decrease the numerical integrator's time step (Δt) as ϕ_p increases. It turns out, however, that numerical stability requires Δt to remain larger than a certain critical value $\Delta t_c(\phi_p,\epsilon)$. We demonstrate in the Appendix that when $\Delta t < \Delta t_c$, the Jacobian matrix of the numerical integrator becomes singular at a certain finite time t. Thus,

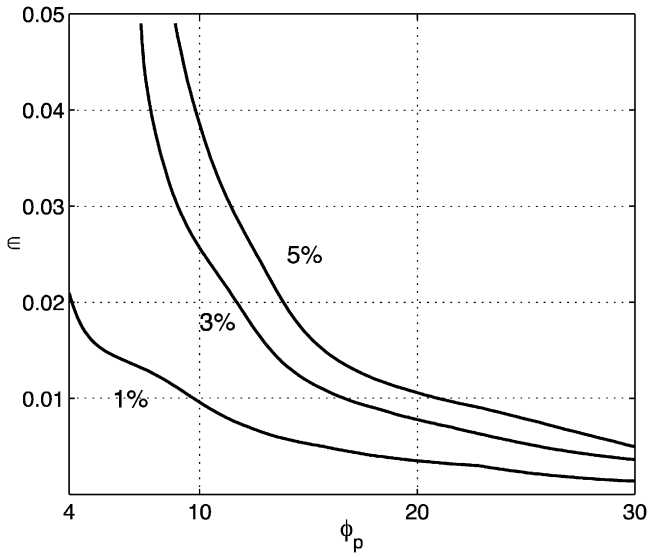

Fig. 4. The range of validity of the approximate model. The domains under the curves correspond to ϕ_p and ϵ values when the discrepancy (E_m) between the approximate and exact predictions is smaller than 1.0%, 3.0%, and 5.0%.

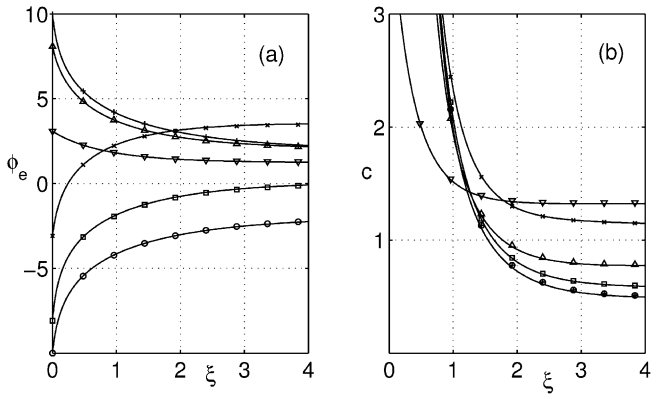

Fig. 5. The potential (a) and concentration (b) in the EDL are depicted as functions of the stretched coordinate ξ at times $t=0$ (○), 0.1 T (□), 0.2 T (×), 0.3 T (▽), 0.4 T (△) and 0.5 T (+). $\phi_p=20$, $\epsilon=0.005$, and $\omega=0.02\,\pi$. The exact solutions are depicted with solid lines and the approximate solutions with symbols.

the numerical solver encounters the conflicting demands of having to maintain small enough time steps to prevent $c^B(-1,t)$ from assuming non-physical, negative values and large enough to avoid a singular Jacobian. These conflicting objectives become increasingly difficult to satisfy as ϕ_p and ϵ increase. Interestingly, the full PNP equations do not experience similar difficulties.

3.2 Alternating Electrode Potential

Next, we consider the case when the electrodes' potentials vary periodically in time:

$$\phi_w(t) = \phi_p \mathrm{Re}\{e^{i\Omega\tau}\} = \phi_p \mathrm{Re}\{e^{i\omega t}\}$$

The dimensionless frequency $\omega = \Omega\lambda_D L/D$. In this case, we have an additional time scale, $\tau_\Omega = 1/\Omega$. When this time scale is smaller than the charge relaxation time of the EDL, $1/\Omega < \lambda_D^2/D$ or $\omega > \epsilon^{-1}$, the EDL does not have time to reach equilibrium. We denote this critical frequency with superscript *, $\omega^* = \epsilon^{-1}$.

When $\phi_p \ll 1$, the approximate model predicts

$$c^B(x,t) \sim 1$$

and

$$\phi_e^B(x,t) \sim \frac{\phi_p x}{2}\left(\frac{e^{-t}}{\omega^2+1} + \frac{\omega\cos(\omega t+\varphi)}{\sqrt{\omega^2+1}}\right), \qquad (37)$$

where $\varphi = \cot^{-1}\omega$. We compared the predictions of the exact and the approximate models with the perturbation solution (37). When $\phi_p \le 2$, $\epsilon = 0.005$ and $\omega = 0.01\omega^*$, all are in a nearly perfect agreement with $E_m < 0.24\%$.

Once initial transients have died out, Figures 5a and 5b depict, respectively, the potential and the concentration inside the EDL as functions of the stretched coordinate ξ at times $t=0$, 0.1T, 0.2T, 0.3T, 0.4T and 0.5T when $\phi_p=20$, $\epsilon=0.005$, and $\omega = 0.02\pi \approx 3\times10^{-4}\omega^*$. Solid lines and symbols represent, respectively, the exact and approximate solutions. The potential and concentration distributions in the EDL vary monotonically, suggesting that at sufficiently low forcing frequencies, the EDL is nearly at equilibrium. This is not surprising, however, since the dimensionless relaxation time of the EDL, $t_D=\epsilon=0.005$, is much smaller than the forcing period $T=2\pi/\omega=100$ and quasi-equilibrium conditions prevail.

Figure 6 compares the predictions of the exact and approximate models as functions of time for the same conditions as in Figure 5. Figs. 6a and 6b depict, respectively, the potential and concentration as functions of time at positions $x=-0.25$, -0.5 and -0.75 during one period. Consistent with Equation 37, the potential field oscillates at the forcing frequency and its amplitude increases linearly with x. The concentration field (Figure 6b) oscillates at double the forcing frequency. This is further exemplified in the phase diagram in Figure 6c. Figure 6c depicts the concentration $c^B(x,t)$ as a function of the potential $\phi_e(x,t)$ at $x=-0.25$, -0.5 and -0.75. Since c is comprised of the sum of the anions and cations' concentrations, it is independent of the sign of the potential, as is reflected in the symmetry of the concentration field with respect to $\phi_e=0$. The alternations of c at double the forcing frequency can be anticipated from the linearized version of Equation 27. Figure 6d depicts the electrode current flux $j(t)$ as a function of the electrodes' potential $\phi_w(t)$. The current is an antisymmetric function of the potential $j(\phi_w(t)) = -j(-\phi_w(t))$. Figure 6e depicts the discrepancy between the exact and approximate (bulk) models' predictions $E(t)$ (Equation 36) as a function of time during one period. In Figure 6, $E_m < 1.0\%$.

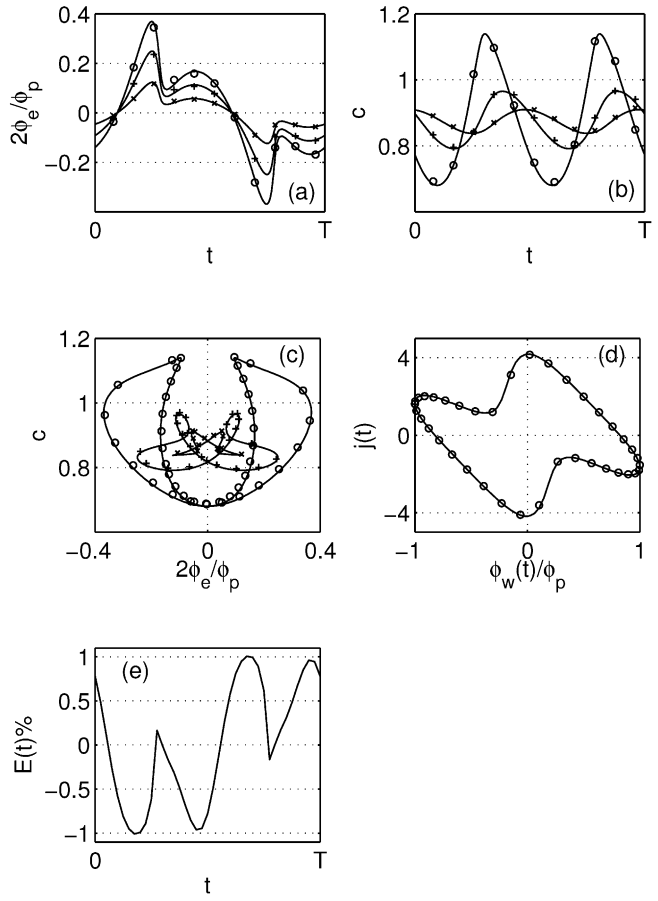

Fig. 6. Comparison between the exact model (solid lines) and approximate model (symbols) predictions. $\phi_p=20$, $\epsilon=0.005$, and $\omega=0.02\,\pi$. The normalized potentials $2\phi_e(x,t)/\phi_p$ (a) and the concentration $c(x,t)$ (b) are depicted as functions of time at $x=-0.25$ (×),-0.5 (+), and -0.75 (○). (c) A phase diagram depicting $c(x,t)$ as a function of $2\phi_e(x,t)/\phi_p$ at various x values. (d) The electrode current as a function of normalized, applied potential $\phi_w(t)/\phi_p$. (e) The discrepancy (%) between the approximate and exact external current as a function of time.

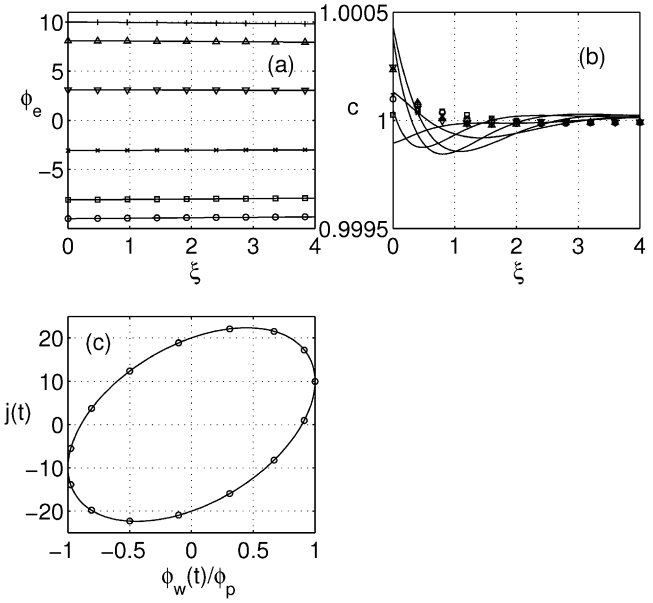

Fig. 7. Comparison of the exact solution (solid lines) and approximate model (symbols) predictions. $\phi_p=2$, $\epsilon=0.005$ and $\omega=2\omega^*$. The potential (a) and concentration (b) are depicted as functions of ξ at times $t=0$ (○), 0.1T (□), 0.2T (×), 0.3T (▽), 0.4T (△), and 0.5T (+). (c) The electrode current as a function of the normalized applied voltage.

Next, we consider high frequencies. Figures 7a and 7b depict, respectively, the potential and concentration in the electric double layer as functions of the stretched coordinate ξ when $\phi_p=20$, $\epsilon=0.005$, and $\omega=400=2\omega^*$ over one half time period. Witness that at this frequency, the EDL does not have time to form. As a result, there no potential drop across the EDL and $\phi_e^B(-1,t)\approx -\phi_w(t)/2$. The exact and approximate models predict qualitatively different concentration profiles (Figure 7b), but the differences between the models' predictions are smaller than 0.05%, which has little effect on electrode current flux (Figure 7c).

To gain further insights, we evaluated the composite solution (26) with small amplitude potential (37). When $\omega\gg1$, once initial transients have died out, the amplitude of the potential alternations in the bulk is proportional to $\omega/\sqrt{\omega^2+1}$ or $O(1)$, while the amplitude of the potential drop across the EDL is proportional to $1/\sqrt{\omega^2+1}$ and diminishes like ω^{-1}. In other words, the potential drop across the EDL is negligible when the dimensionless frequency $\omega\gg1$. Therefore, we expect the composite solution to provide reasonable estimates of the external current both when the frequency is low (when the EDL is at quasi-equilibrium) and when the frequency is high (no EDL).

We repeated similar computations to the ones presented in Figure 6 and Figure 7 for various frequencies and electrode potentials ϕ_p. Figure 8a depicts the error (36) as a function of the frequency when $\phi_p=6$, 14 and 30. $\epsilon=0.001$. Figure 8b shows error contours as functions of ω and ϕ_p. Figure 9a depicts the error (Equation 38) as a function of the normalized frequency when $\phi_p=2$, 10, and 20. $\epsilon=0.005$. Figure 9b shows error contours as functions of ω and ϕ_p. When $\omega>10$, the bulk solution provides an excellent approximation.

4 Conclusions

The modeling of various systems of current interest, ranging from electrochemical energy storage devices to desalination reactors to colloidal systems, requires the numerical solution of the time-dependent Poisson-Nernst-Planck (PNP) equations in three-dimensions and/or in complex geometries (such as porous electrodes). The computational task of solving the PNP equations is challenging due to the presence of disparate length scales, such as the Debye screening length and the diffusion length, and disparate device dimensions. In particular, the need to resolve the electric double layers poses a significant demand on computational resources. When the temporal variations in the

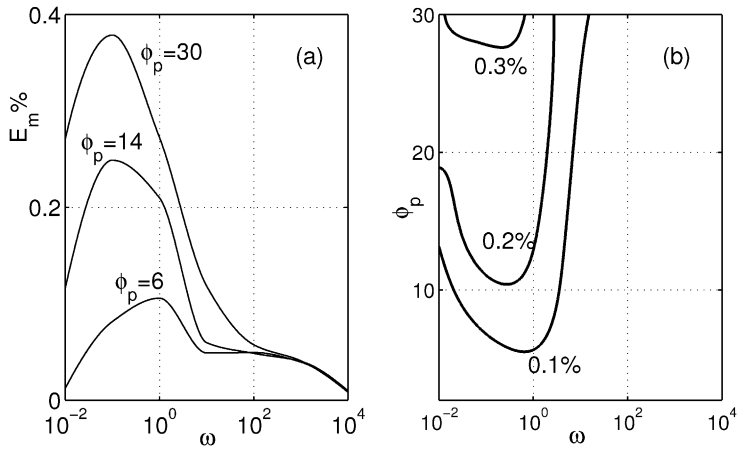

Fig. 8. (a) The error E_m as a function of the frequency ω. (b) Contours of constant error $E_m = 0.1\,\%$, $0.2\,\%$, and $0.3\,\%$ as functions of ω and ϕ_p. $\epsilon = 0.001$.

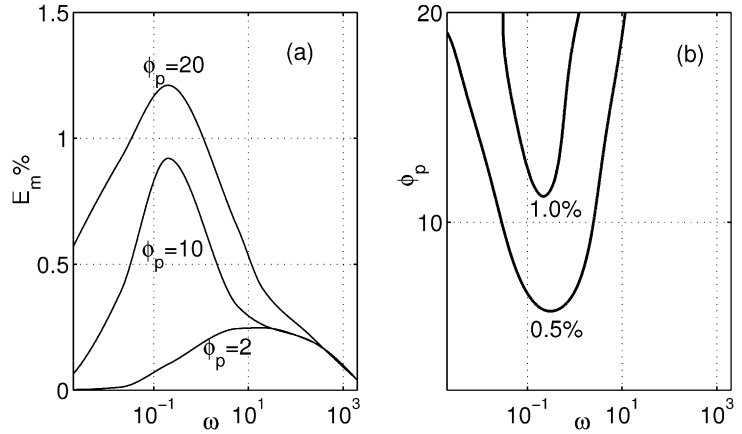

Fig. 9. (a) The error E_m as a function of the frequency ω and (b) contours of constant error $E_m = 0.5\,\%$ and $E_m = 1.0\,\%$ as functions of ω and ϕ_p. $\epsilon = 0.005$.

electrodes' potentials are relatively slow, the computational burden can be greatly reduced by assuming that the EDLs are at quasi-equilibrium and the bulk of the electrolyte solution retains electro neutrality. To assess the error incurred when applying the quasi-equilibrium approximation, we compared the predictions of the Poisson-Nernst-Planck equations with the predictions of a simplified bulk model that replaces the charge and ion accumulation in the EDL with appropriate boundary conditions. The comparison was carried out for a one-dimensional electrolytic cell confined between two blocking (perfectly polarizable) electrodes, both when the electrodes' potential difference was subjected to a step change and when it was subjected to time-periodic alternations. Although the approximate model is well known, a systematic study of its range of validity appears to be lacking.

In the case of a step change, when the EDL thickness is small and the electrodes' potential difference moderate, the approximate solution is in excellent agreement with the exact one. The error associated with the use of the approximate solution was determined as a function of the relative Debye screening length and the electrodes' potential. The discrepancy between the exact and approximate solutions increases as the thickness of the EDL and the magnitude of the potential difference increase.

In the case of periodic alternations in electrode potential, in addition to the thickness of the EDL and the width of the electrolytic cell, a third length scale comes into play – the diffusion penetration depth. We denote with ω^* the frequency when the diffusion penetration depth is comparable to the thickness of the Debye screening length. We calculated the error associated with the approximate solution as a function of the electric potential amplitude and frequency. When the frequency is small, the EDL can be considered as being at quasi-equilibrium and the approximate model predictions are in reasonable agreement with the exact ones. At high frequencies, $\omega \geq 10$, the potential and concentration variations in the EDL are negligible. Thus, the approximate model (the bulk solution) provides a good approximation to the exact one.

Appendix

To examine the roots of the instability in the numerical solution of the bulk model, we constructed an approximate model of the bulk Equations 20 and 21 with boundary conditions (24) and (25). The model is sufficiently simple to enable us to expose the numerical instability while still retaining the essential physics of the process.

At moderate times $t \ll \epsilon^{-1/2}$, we approximate the flux at $x=-1$ as predicted by the bulk model (20) with the integral equation ([14] page 133 Equation 3)

$$\left[\frac{\partial c^B(x,t)}{\partial x}\right]_{x=-1} = -\frac{1}{\sqrt{\pi\epsilon}}\int_0^t \frac{\dot{c}_1(\tau)}{\sqrt{t-\tau}}\mathrm{d}\tau. \tag{A1}$$

In the above, $c_1(t) = c^B(-1,t)$ and $\dot{c}_1 = {\mathrm{d}c_1}/{\mathrm{d}t}$. As we shall see shortly, (A1) provides an excellent approximation of (20). Next, we replace the LHS of (A1) with the boundary condition (24) to obtain

$$\frac{\mathrm{d}}{\mathrm{d}t}\left[4\sqrt{c_1}\sinh^2\left(\frac{\frac{\phi_p}{2}+\phi_1}{4}\right)\right] = \frac{-1}{\sqrt{\pi\epsilon}}\int_0^t \frac{\dot{c}_1(\tau)}{\sqrt{t-\tau}}\mathrm{d}\tau \tag{A2}$$

where $\phi_1 = \phi_e^B(-1,t)$. We integrate the potential Equation 21 once and apply the boundary condition (25) to obtain

$$\frac{\mathrm{d}}{\mathrm{d}t}\left[-2\sqrt{c_1}\sinh\left(\frac{-\frac{\phi_p}{2}-\phi_1}{2}\right)\right] = \phi_1. \tag{A3}$$

In the above, we approximate $c^{\mathrm{B}} \approx 1$ and $\partial\phi_e{}^{\mathrm{B}}(-1,t)/\partial x \approx \phi_e{}^{\mathrm{B}}(-1,t) = \phi_1$. The latter is justified since the profile for ϕ_e^B is nearly a linear function of x, as is evident in Figure 3.

Next, we integrate the non-linear ODEs (A2–A3) with the initial conditions $c_1(0)=1$ and $\phi_1(0)=-\phi_p/2$. At early times $t \ll 1$, the solutions can be expanded in time t.

$$c_1(t) = 1 - \frac{\phi_p^2}{6}\sqrt{\frac{\epsilon}{\pi}}\,t^{3/2} + O\left(t^{5/2}\right)$$

and

$$\phi_1(t) = -\frac{\phi_p}{2} + \frac{\phi_p}{2}t - \frac{\phi_p}{4}t^2 + \frac{\phi_p^3}{24}\sqrt{\frac{\epsilon}{\pi}}\,t^{5/2} + O\left(t^3\right). \tag{A4}$$

The short time solution will provide us with the initial conditions needed for the numerical scheme.

To obtain finite-time solutions, we resort to a numerical method. To simplify notation, we introduce the new variable

$$y = \frac{\phi_p}{4} + \frac{\phi_1}{2}$$

and recast the system (A3) and (A2) into

$$(\sqrt{c_1}\cosh y)\dot{y} + \frac{\sinh y}{2\sqrt{c_1}}\dot{c}_1 = \frac{\phi_p}{4} - y \tag{A5}$$

$$(\sqrt{c_1}\sinh y)\dot{y} + \frac{\sinh^2(y/2)}{\sqrt{c_1}}\dot{c}_1 = \frac{-1}{2\sqrt{\pi\epsilon}}\int_0^t \frac{\dot{c}_1(\tau)}{\sqrt{t-\tau}}\mathrm{d}\tau \tag{A6}$$

The solutions of (A5) and (A6) are evaluated at discrete time instants $t = t_k (k = 0,1,2,\ldots)$ with $t_0 = 0$. For simplicity, we employ uniform time steps Δt, i.e., $t_k = k\Delta t$. The integral in (A6) is first manipulated to remove the singularity at time $t = t_n$ and then approximated with the trapezoidal rule.

$$\int_0^{t_n} \frac{\dot{c}_1(\tau)}{\sqrt{t_n-\tau}}\mathrm{d}\tau = \int_0^{t_n} \frac{\dot{c}^{(n)} - \dot{c}^{(n)} + \dot{c}_1(\tau)}{\sqrt{t_n-\tau}}\mathrm{d}\tau = \dot{c}^{(n)}2\sqrt{t_n} + \int_0^{t_n} \frac{\dot{c}_1(\tau) - \dot{c}^{(n)}}{\sqrt{t_n-\tau}}\mathrm{d}\tau$$

$$= \sqrt{\Delta t}\left(2\sqrt{n}\dot{c}^{(n)} + \frac{\dot{c}^{(0)} - \dot{c}^{(n)}}{2\sqrt{n}} + \frac{\dot{c}^{(1)} - \dot{c}^{(n)}}{\sqrt{n-1}} + \cdots + \frac{\dot{c}^{(n-1)} - \dot{c}^{(n)}}{\sqrt{1}}\right)$$

$$= \sqrt{\Delta t}\left(\alpha^{(n)}\dot{c}^{(n)} + \beta^{(n)}\right), \tag{A7}$$

where $\dot{c}^{(n)} = \dot{c}_1(t_n)$

$$\alpha^{(n)} = 2\sqrt{n} - \frac{1}{2\sqrt{n}} - \frac{1}{\sqrt{n-1}} - \cdots - 1,$$

$$\beta^{(n)} = \frac{\dot{c}^{(0)}}{2\sqrt{n}} + \frac{\dot{c}^{(1)}}{\sqrt{n-1}} + \cdots + \frac{\dot{c}^{(n-1)}}{\sqrt{1}} \tag{A8}$$

Note that $\alpha^{(n)}$ is bounded and converges quickly to $\lim_{n\to\infty}\alpha^{(n)} = 1.4604$. The discretized form of Equations A5 and A6 is, therefore

$$\begin{pmatrix} \dot{y}^{(n)} \\ \dot{c}^{(n)} \end{pmatrix} = \mathbf{A}^{-1}\begin{pmatrix} \frac{\phi_p}{4} - y^{(n)} \\ -\frac{1}{2}\sqrt{\frac{\Delta t}{\pi\epsilon}}\,\beta^{(n)} \end{pmatrix} \tag{A9}$$

where

$$\mathbf{A} = \begin{pmatrix} \sqrt{c^{(n)}}\cosh y^{(n)} & \frac{1}{2\sqrt{c^{(n)}}}\sinh y^{(n)} \\ \sqrt{c^{(n)}}\sinh y^{(n)} & \frac{1}{\sqrt{c^{(n)}}}\sinh^2(y^{(n)}/2) + \frac{a^{(n)}}{2}\sqrt{\frac{\Delta t}{\pi\epsilon}} \end{pmatrix}$$

The system (A9) can be integrated by a simple predictor-corrector scheme. To start the calculation, the initial values of the solution (when $n=0$ and 1) are obtained from (A4).

Figure 10 compares the solutions of the simplified model (A2-A3) and the finite element solution of the bulk Equations 20 and 21 (computed with COMSOL) when the electrode potential is subjected to a step change

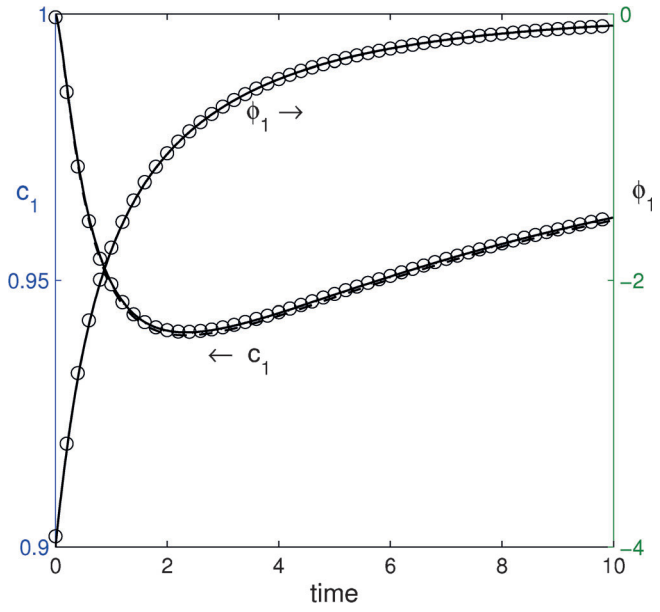

Fig. 10. Comparison of the COMSOL solution for the bulk equations (○, $\Delta t = 0.01$) and the solutions of the ODE model (solid lines $\Delta t = 0.01$, dotted lines $\Delta t = 0.02$, and dashed lines $\Delta t = 0.05$) for the step change in electrode potential $\phi_p = 8$, and $\epsilon = 0.001$.

$\phi_p = 8$ and $\epsilon = 0.001$. When $0.01 \le \Delta t \le 0.05$, the solutions of the simplified model converge and are in excellent agreement with the finite element solution of the bulk equations.

However, when a smaller time step was used in solving the simplified model, numerical instabilities occurred. Figure 11 depicts the solutions computed with $\Delta t = 0.001$ (solid line) and otherwise identical parameters as in Figure 10. For comparison, Figure 11a also depicts the converged solution with $\Delta t = 0.01$ (dashed line). When $\Delta t = 0.001$, the solutions exhibit non-physical oscillations in the time derivatives $\dot{c}_1$ and $\dot{y}$ (Figure 11b) and a transition to a physically inadmissible branch (e.g. $c_1 > 1$ or $c_1 < 0$) at time $t_s \approx 1.59$. The time t_s for the onset of the instability decreases as the time step Δt decreases. This numerical instability is present even at small electrode potentials. For example, when $\phi_p = 2$, $\epsilon = 0.01$, and $\Delta t = 10^{-4}$, the instability occurs at $t_s \approx 1.07$; and when $\phi_p = 1$, $\epsilon = 0,01$, and $\Delta t = 10^{-5}$, the instability occurs at $t_s \approx 1.24$. At these small electrode potentials, the solutions of Equations A8 converge readily when larger time steps are used. This numerical instability is not unique to the particular form of discretization (A8) and was present when various other numerical integration schemes were experimented with. In fact, the instability was also present in the COMSOL solution of the bulk Equations 20 and 21 when a small time step $\Delta t = 0.001$ was used for the case shown in Figure 10.

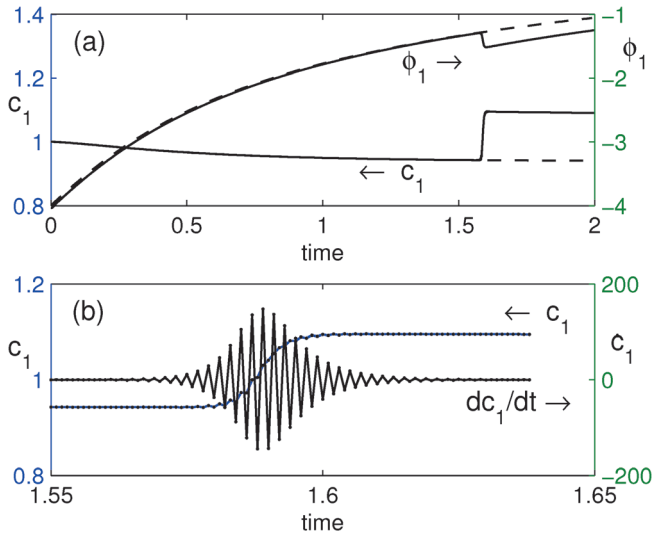

Fig. 11. (a) Solutions from the ODE model with time step $\Delta t = 0.001$ (solid lines) for the same case as in Figure A1. Dashed lines represent the converged solution with $\Delta t = 0.01$. (b) Zoom-in view of the concentration c_1 and its time derivative $\dot{c}_1$ around the numerical instability.

The origins of the instability can be readily identified by examining the determinant of the matrix **A** in (A9),

$$\det\mathbf{A} = -\sinh^2(y/2) + \frac{\alpha^{(n)}}{2}\sqrt{\frac{\Delta t}{\pi\epsilon}c_1}\cosh y,$$

The first term of det**A** is always negative and the second term is always positive since $\alpha^{(n)} \approx 1.4604$. Thus, det**A** can become singular and non-invertible as the solution (c_1, y) evolves. Estimating the critical Δt value needed to assure stability and the time t_s when instability occurs is complicated by the non-linearity as both y and c_1 vary during the solution process.

It is instructive to consider a limiting case of small electrode potentials. When $\phi_p \ll 1$, the problem admits the asymptotic solution (35) and (34): $c_1 \approx 1$ and $y \approx \frac{\phi_p}{4}(1 - e^{-t})$. With the above expression, det**A** = 0 when

$$t_{\text{det}} = -\ln\left[1 - \frac{4}{\phi_p}\sqrt{2\alpha^{(n)}}\left(\frac{\Delta t}{\pi\epsilon}\right)^{\frac{1}{4}}\right] \qquad \text{(A10)}$$

Equation A10 indicates that numerical stability requires $\Delta t > \Delta t_c \sim 1.4 \times 10^{-3}\epsilon\phi_p^4$. When $\Delta t < \Delta t_c$, there is always a finite time t_{det} when **A** becomes singular, and the numerical integration of (A9) runs into difficulties.

The numerical instability observed in the solution of the simplified model is very similar to the one observed in the finite element solution of the bulk equations. After the finite element discretization of the bulk equations, the stiffness matrix that corresponds to the variables at the boundary node has the same form as the matrix **A** (Equation A9). It should be pointed out that this instability is unique to the nonlinear system (20–21) with particular boundary conditions (24–25), and the solution to the full PNP equations does not experience the similar instability.

Acknowledgements

The work was supported, in part, by the State of Pennsylvania's Ben Franklin Technology Development Authority – the Energy Commercialization Institute (ECI).

References

[1] P. M. Biesheuvel, M. Z. Bazant, *Phys. Rev. E, Statist. Nonlin. Soft Mat. Phys.* **2010**, *81*, 031502.
[2] M. Duduta, B. Ho, V. C. Wood, P. Limthongkul, V. E. Brunini, W. C. Carter, Y. Chiang, *Adv. Energy Mater.* **2011**, *1*, 511–516.
[3] A. Johnson, J. Newman, *J. Electrochem. Soc.* **1971**, *118*, 510–517.
[4] J. Newman, W. Tiedemann, *AIChE J.* **2004**, *21*, 25–41.
[5] V. Presser, C. R. Dennison, J. Campos, K. W. Knehr, E. C. Kumbur, Y. Gogotsi, *Adv. Energy Mater.* **2012**, *2*, 895–902.
[6] M. S. Kilic, M. Z. Bazant, A. Ajdari, *Phys. Rev. E, Statist. Nonlin. Soft Mat. Phys.* **2007**, *75*, 021502.
[7] M. S. Kilic, M. Z. Bazant, A. Ajdari, *Phys. Rev. E, Statist. Nonlin. Soft Mat. Phys.* **2007**, *75*, 021503.
[8] J. S. Newman, C. W. Tobias, *J. Electrochem. Soc.* **1962**, *109*, 1183–11191.
[9] Y. K. Suh, S. Kang, *Phys. Rev. E, Statist. Nonlin. Soft Mat. Phys.* **2008**, *77*, 031504.
[10] M. Z. Bazant, K. Thornton, A. Ajdari, *Phys. Rev. E Statist. Nonlin. Soft Mat. Phys.* **2004**, *70*, 021506-1-021506-24.
[11] L. Højgaard Olesen, M. Z. Bazant, H. Bruus, *Phys. Rev. E Statist. Nonlin. Soft Mat. Phys.* **2010**, *82*, 011501.
[12] D. L. Chapman, *Philosoph. Mag. Ser. 6* **1913**, *25*, 475–481.
[13] G. Gouy, *J. Phys.* **1910**, *9*, 457–467.
[14] R. V. Churchill, *Operational Mathematics*, McGraw-Hill, **1958**.

Received: August 1, 2014
Accepted: October 26, 2014
Published online: January 28, 2015

